On the Adhesive JKR Contact and Rolling Models for Reduced Particle Stiffness Discrete Element Simulations

Hærvig, Jakob; Kleinhans, Ulrich; Wieland, Christoph; Spliethoff, Hartmut; Jensen, Anna Lyhne; Sørensen, Kim; Condra, Thomas Joseph

On the Adhesive JKR Contact and Rolling Models for Reduced Particle Stiffness Discrete Element Simulations

J. Hærvig[a,*], U. Kleinhans[b], C. Wieland[b], H. Spliethoff[b], A.L. Jensen[a], K. Sørensen[a], T.J. Condra[a]

[a]*Aalborg University, Department of Energy Technology, Pontoppidanstræde 111, DK-9220 Aalborg, Denmark*
[b]*Technical University of Munich, Institute of Energy Systems, Boltzmannstraße 15, DE-85748 Garching, Germany*

Abstract

Discrete Element Method (DEM) simulations are a promising approach to accurately predict agglomeration and deposition of micron-sized adhesive particles. However, the mechanistic models in DEM combined with high particle stiffness for most common materials require time step sizes in the order of nano seconds, which makes DEM simulations impractical for more complex applications.

In this study, analytically derived guidelines on how to reduce computational time by using a reduced particle stiffness are given. The guidelines are validated by comparing simulations of particles with and without reduced particle stiffness to experimental data. Then two well-defined test cases are investigated to show the applicability of the guidelines.

When introducing a reduced particle stiffness in DEM simulations by reducing the effective Young's modulus from E to E_{mod}, the surface energy density γ in the adhesive Johnson-Kendall-Roberts (JKR) model by Johnson et al. [1] should be modified as $\gamma_{\mathrm{mod}} = \gamma \left(E_{\mathrm{mod}}/E\right)^{2/5}$. Using this relation, the stick/rebound threshold remains the same but the collision process takes place over a longer time period, which allows for a higher time step size. When rolling motion is important, the commonly used adhesive rolling resistance torque model proposed by Dominik and Tielens [2, 3], Krijt et al. [4] can be used by modifying the contact radius ratio $(a/a_0)^{3/2}$ to $(a_{\mathrm{mod}}/a_{0,\mathrm{mod}})^{3/2}$, whilst keeping the other terms unaltered in the description of the rolling resistance torque $M_{\mathrm{r,mod}} = -4F_{\mathrm{C}} \left(a/a_0\right)^{3/2} \xi$. Furthermore, as the particle stiffness is reduced from E to E_{mod}, the time period for collisions (or oscillations when particles stick upon impact) Δt_{col} is found to vary as $\Delta t_{\mathrm{col,mod}} = \Delta t_{\mathrm{col}}(E/E_{\mathrm{mod}})^{2/5}$. As the collision duration and the collision time step size are directly related, this criterion can be used to estimate how much the time step size can be changed as a reduced particle stiffness is introduced.

Introducing particles with a reduced particle stiffness has some limitations when strong external forces are acting to break-up formed agglomerates or re-entrain particles deposited on a surface out into the free stream. Therefore, care should be taken in flows with high local shear to make sure that an external force, such as a fluid drag force, acting to separate agglomerated particles, is several orders of magnitude lower than the critical force required to separate particles.

Keywords: Discrete Element Method, Reduced particle stiffness, Adhesive particles, JKR adhesive model, Rolling resistance torque, Computational efficiency

1. Introduction

Discrete Element Method (DEM) simulations are typically used to accurately predict the motion of particles in systems with high local particle volume fraction where particle-particle collisions are important. Recently, the motion of adhesive particles has received increased attention [5] due to the wide range of applications which include, but are not limited to, particulate fouling layers in heat exchangers, food processing, sediment transport, aerosol modelling, fluidized beds and dust coagulating to form early stages of planets in space. As opposed to other methods, DEM simulations resolve particle-particle collisions directly using a mechanistic approach. As each particle-particle collision is resolved over numerous time steps, the required computational time is high compared to other methods [6]. A widely used approach to decrease computational costs is to decrease the particle stiffness, namely Young's modulus, and thereby make collisions take place over longer time periods allowing for an increased time step size. For collisions involving non-adhesive particles, numerous studies suggest that the particle stiffness can be reduced by several orders of magnitude without altering the collisions in terms of separating velocity after collision [7, 8]. However, when introducing adhesive particles, recent studies have pointed out that a reduced particle stiffness has to be balanced by a reduced adhesive force. Therefore, Kobayashi et al. [9]

---
*Corresponding author: Tel.: +45 22508131
Email address: jah@et.aau.dk (J. Hærvig)

introduced a dynamic van der Waals adhesion model upon collision that scales the adhesive force F_ad according to the square root of the ratio of particle spring constants k as: $F_\text{ad,mod}/F_\text{ad} = \sqrt{k_\text{mod}/k}$, where subscript *mod* denotes modified values. Gu et al. [8] extended the work and included the fact that the van der Waals force is effective over a finite distance before the particles come into physical contact. Common for these studies is the fact that they assume particle deformation to play a negligible role on the adhesive force upon collision. This assumption is valid for sufficiently small particles, where particle deformation is negligible [10].

When the particle diameter is large (typically $d_\text{p} > 10$ µm), particle deformation cannot be neglected when describing the adhesive force. The importance of particle deformation on the adhesive behaviour is described by Tabor [11] through the dimensionless Tabor parameter λ_T where R, γ, E and D_min define effective particle radius, surface energy density, effective Young's modulus and minimum atomic separation distance between particles (typically taken to be 1.65 Å [12, 13]):

$$\lambda_\text{T} = \left(\frac{4R\gamma^2}{E^2 D_\text{min}^3} \right)^{1/3} \tag{1}$$

$$\frac{1}{R} = \frac{1}{r_\text{i}} + \frac{1}{r_\text{j}}, \qquad \frac{1}{E} = \frac{1-\nu_\text{i}^2}{E_\text{i}} + \frac{1-\nu_\text{j}^2}{E_\text{j}} \tag{2}$$

where r and ν refer to particle radius and Poisson's ratio respectively and subscripts i and j refer to particle i, j. The study by Johnson and Greenwood [10] shows that the adhesive Johnson-Kendall-Roberts (JKR) model by Johnson et al. [1] is valid for $\lambda_\text{T} > 3$, the Derjaguin-Muller-Toporov (DMT) model by Derjaguin et al. [14] is valid for $\lambda_\text{T} < 0.1$ and the model by Maugis [15] is valid in between the two when $0.1 \leq \lambda_\text{T} \leq 3$.

With an increasing number of studies on collisions of adhesive particles being carried out, the aim of this paper is to emphasise the importance of reducing the particle adhesiveness when a reduced particle stiffness is introduced. For this purpose an analytically derived criterion on how to adjust the surface energy density to account for a reduced particle stiffness for collisions in the JKR limit ($\lambda_\text{T} > 3$) is presented. This paper is structured as follows: Firstly, the adhesive DEM modelling framework is briefly outlined. Secondly, the criterion on how to reduce particle stiffness is presented for both collisions and rolling behaviour. Thirdly, numerical simulations of adhesive particles are compared to experimental data found in literature. Lastly, two simple test cases are investigated in more details to show the applicability of the proposed criterion. These test cases represent types of collisions commonly encountered in the particle agglomeration and deposition processes:

1. Binary head-on adhesive particle/particle or particle/wall collisions forming agglomerates or deposition.

2. Collisions of single adhesive particles with a wall. Here the particles are affected by a constant external force parallel to the wall (e.g. a gravity force, time-independent fluid force or a constant magnetic force). Here focus is on the rolling resistance torque, which causes particles to stick to a surface, despite being affected by a constant force.

2. Modelling Framework

The translational and rotational motion of particles is obtained using the DEM, where Newton's equation of motion is solved to obtain the instantaneous translational and rotational position for each particle:

$$m\frac{\text{d}^2\boldsymbol{x}}{\text{d}t^2} = \boldsymbol{F}_\text{con} + \boldsymbol{F}_\text{ext} \tag{3}$$

$$I\frac{\text{d}\boldsymbol{\omega}}{\text{d}t} = \boldsymbol{M}_\text{con} + \boldsymbol{M}_\text{r} \tag{4}$$

where the forces contributing are the contact force upon impact $\boldsymbol{F}_\text{con}$ and an external force $\boldsymbol{F}_\text{ext}$ which could represent a gravity force, a time-independent fluid force or a constant magnetic force. Likewise, the total torque is the sum of a contact torque $\boldsymbol{M}_\text{con}$ and a rolling resistance torque $\boldsymbol{M}_\text{r}$. The contact force is split into normal and tangential contributions ($\boldsymbol{F}_\text{con,n}$ and $\boldsymbol{F}_\text{con,t}$), where the normal contact force is the sum of a spring force, an adhesive force and a damping force contribution:

$$\boldsymbol{F}_\text{con,n} = \boldsymbol{F}_\text{spring,n} + \boldsymbol{F}_\text{jkr,n} + \boldsymbol{F}_\text{damp,n} \tag{5}$$

In the tangential direction, spring and damping force contributions are taken into account through:

$$\boldsymbol{F}_\text{con,t} = \boldsymbol{F}_\text{spring,t} + \boldsymbol{F}_\text{damp,t} \tag{6}$$

Figure 1 gives an overview of the force contributions acting on a particle upon collision with another particle (partly shown on the left).

2.1. Adhesive contact between particles and a surface

Numerous approaches have been suggested to account for an adhesive force. Common for the approaches is that they rely on a surface energy density γ to describe the adhesive force. For small λ_T, the contact independent van der Waals formulation by Hamaker [16] is used in studies such as [8, 9, 17, 18] to account for the adhesive force. For higher λ_T (softer particles), the contact dependent adhesive JKR force proposed by Johnson et al. [1] is used in studies such as [19, 20]. In the present study, focus is on the simplified JKR model suited for DEM simulations and used in studies such as [13, 21, 22]. The simplified JKR model has the same force-displacement relation as the original model, requires the same 8/9 of the critical force $F = (8/9)F_\text{C} = (8/9)3\pi R\gamma$ to break contact but assumes contact is broken as soon as the normal overlap becomes negative in the particle separation process. At
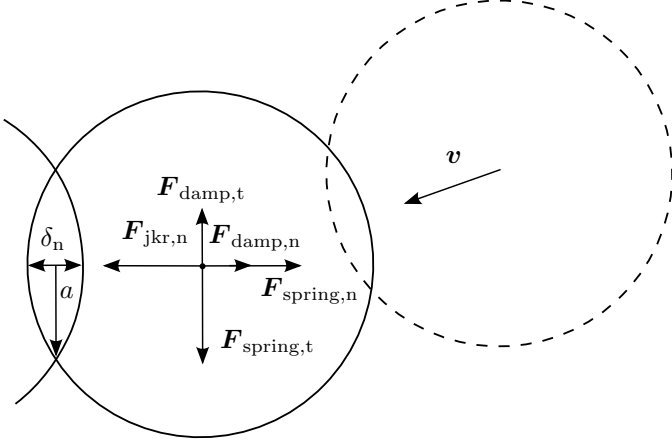
Figure 1: Illustration of contact forces upon collision of two adhesive particles shown with solid black lines. The particles are still approaching each other so that the normal damping force points in the direction opposite of motion.

equilibrium condition when the adhesive force balances the spring force, the contact radius is given by [23]:

$$a_0 = \left(\frac{9 \pi \gamma R^2}{E} \right)^{1/3} \qquad (7)$$

as in the original JKR model. The normal spring force described by the Hertzian contact model is modified as follows due to an adhesive force:

$$\boldsymbol{F}_{\mathrm{jkr,n}} = 4\sqrt{\pi \gamma E a^3} \boldsymbol{n} \qquad (8)$$

$$\boldsymbol{F}_{\mathrm{spring,n}} = -\frac{4E}{3R} a^3 \boldsymbol{n} \qquad (9)$$

where the relation between contact radius a and normal overlap δ_{n} (see figure 1) for adhesive JKR contact is given by [13, 22]:

$$a^4 - 2R\delta_{\mathrm{n}} a^2 - \frac{4\pi\gamma}{E} R^2 a + R^2 \delta_{\mathrm{n}}^2 = 0 \qquad (10)$$

which can be solved using an iterative approach or the analytical expression derived by Parteli et al. [13]. Furthermore, a normal damping force contributes to the contact normal force by dissipating kinetic energy in the particle material:

$$\boldsymbol{F}_{\mathrm{damp,n}} = -2\frac{5}{6}\beta \sqrt{S_{\mathrm{n}} m} \boldsymbol{v}_{\mathrm{n}} \qquad (11)$$

where β accounts for the energy lost upon collision through the coefficient of restitution e while S_{n} takes the particle properties into account:

$$\beta = \frac{\ln (e)}{\sqrt{\ln^2 (e) + \pi^2}} \qquad (12)$$

$$S_{\mathrm{n}} = 2E\sqrt{R\delta_{\mathrm{n}}} \qquad (13)$$

where m is particle mass, v_{n} is the relative normal velocity, and $\boldsymbol{n}$ is the normal unit vector. In the tangential

direction, the spring force contribution is:

$$\boldsymbol{F}_{\mathrm{spring,t}} = -S_{\mathrm{t}} \Delta s_{\mathrm{t}} \qquad (14)$$

where Δs_{t} is tangential displacement between the particles and $S_{\mathrm{t}} = 8G\sqrt{R\delta_{\mathrm{n}}}$ with the effective shear modulus G:

$$\frac{1}{G} = \frac{2 - \nu_{\mathrm{i}}}{G_{\mathrm{i}}} + \frac{2 - \nu_{\mathrm{j}}}{G_{\mathrm{j}}} \qquad (15)$$

Where the shear moduli for particle i,j are related to the Young's modulus through $G_{\mathrm{i}} = E_{\mathrm{i}}/(2(1 + \nu_{\mathrm{i}}))$ and $G_{\mathrm{j}} = E_{\mathrm{j}}/(2(1 + \nu_{\mathrm{j}}))$. Likewise, energy is dissipated in the tangential direction by a damping force:

$$\boldsymbol{F}_{\mathrm{damp,t}} = -2\sqrt{\frac{5}{6}}\beta \sqrt{S_{\mathrm{t}} m} \boldsymbol{v}_{\mathrm{t}} \qquad (16)$$

where $\boldsymbol{v}_{\mathrm{t}}$ is the relative tangential velocity of the particles. In the case of adhesive contact, the tangential force is truncated to fulfil [24, 25]:

$$|\boldsymbol{F}_{\mathrm{con,t}}| \leq \mu_{\mathrm{s}} |F_{\mathrm{N}} + 2F_{\mathrm{C}}| \qquad (17)$$

where μ_{s} is the sliding friction coefficient.

2.2. Adhesive rolling, sliding and twisting resistance

To predict the formation of agglomerates or particles sticking to a wall, a description of adhesive rolling plays a major role [2–4]. Due to the small particle inertia of micron-sized particles, twisting (rotation along the axis connecting two particles) and sliding (relative tangential motion without rotation) are less important than rolling, to accurately predict formation/break-up of agglomerates [19, 26]. Therefore, focus is on the adhesive rolling behaviour and how to modify the adhesive rolling resistance model to account for the reduced particle stiffness.

When a particle is in normal equilibrium with a wall, the centre of contact and projected centre of gravity are coincident, see figure 2(a). However, when an external force $\boldsymbol{F}_{\mathrm{ext}}$ is applied, a small shift between the centre of contact and projected centre of gravity will build up, as illustrated in figure 2(b). The result of this asymmetric contact region is a torque $\boldsymbol{M}_{\mathrm{r}}$ opposing rotation and trying to obtain the symmetric contact region as in figure 2(a). If the particle is rolled less than a critical rolling distance ($\xi < \xi_{\mathrm{crit}}$), the particle rolls back to obtain the same contact point when the external force is removed. However, when the particle is rolled a distance longer than the critical rolling displacement ($\xi > \xi_{\mathrm{crit}}$), the particle is moved irreversibly. While Dominik and Tielens [2, 3] suggest a critical rolling displacement in the order of an atom diameter, the more recent study by Krijt et al. [4] relates the critical rolling displacement to the equilibrium contact radius a_0 and a material dependent adhesion hysteresis parameter $\Delta\gamma/\gamma$ to obtain improved experimental agreement through:

$$\xi_{\mathrm{crit}} = \frac{a_0}{12} \frac{\Delta\gamma}{\gamma} \qquad (18)$$
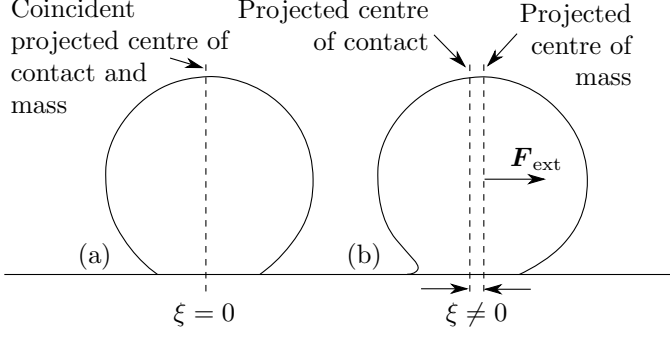
3

Figure 2: Adhesive particle in contact with a wall and in normal equilibrium ($\boldsymbol{F}_{\mathrm{jkr,n}} = \boldsymbol{F}_{\mathrm{spring,n}}$): (a) Zero force applied results in particle centre of mass and centre of contact being coincident; (b) An external force applied $\boldsymbol{F}_{\mathrm{ext}} \neq \boldsymbol{0}$ results in a non-coincident projected centre of mass and centre of contact.

In general as a particle rolls, the rolling displacement ξ is obtained by integrating the rolling velocity:

$$\xi = \left(\int_{t_0}^{t_1} \boldsymbol{v}_{\mathrm{L}}(t) \mathrm{d}t \right) \cdot \boldsymbol{t}_{\mathrm{r}} \tag{19}$$

where the rolling velocity $\boldsymbol{v}_{\mathrm{L}}$ is defined as:

$$\boldsymbol{v}_{\mathrm{L}} = R \left(\boldsymbol{\omega}_{\mathrm{i}} - \boldsymbol{\omega}_{\mathrm{j}} \right) \times \boldsymbol{n} + \frac{1}{2} \frac{r_{\mathrm{i}} - r_{\mathrm{j}}}{r_{\mathrm{i}} + r_{\mathrm{j}}} \boldsymbol{v}_{\mathrm{S}} \tag{20}$$

which can conveniently be implemented into the DEM method by incremental changes between two successive time steps. The rolling resistance torque is then given by [2, 3]:

$$M_{\mathrm{r}} = \begin{cases} k_{\mathrm{r}} \xi & \text{if } \xi < \xi_{\mathrm{crit}} \\ k_{\mathrm{r}} \xi_{\mathrm{crit}} & \text{if } \xi \geq \xi_{\mathrm{crit}} \end{cases} \tag{21}$$

with rolling stiffness $k_{\mathrm{r}} = 4 F_{\mathrm{C}} \left(a/a_0 \right)^{3/2}$. As the rolling displacement ξ cannot exceed the critical rolling displacement ξ_{crit}, the rolling displacement is numerically truncated to fulfil:

$$|\xi| \leq |\xi_{\mathrm{crit}}| \tag{22}$$

3. Reduced Particle Stiffness

3.1. Modified adhesive JKR model for reduced particle stiffness

When a reduced particle stiffness is introduced in DEM simulations, the particles will inevitably overlap more during collision. If the surface energy density γ is left unchanged, the result is a more adhesive collision as the kinetic energy lost upon collision is increased significantly. Therefore, a reduced particle stiffness has to be balanced by a reduced surface energy density for the outcome of the collision to remain the same. For the separation energy required to separate two particles in contact to remain
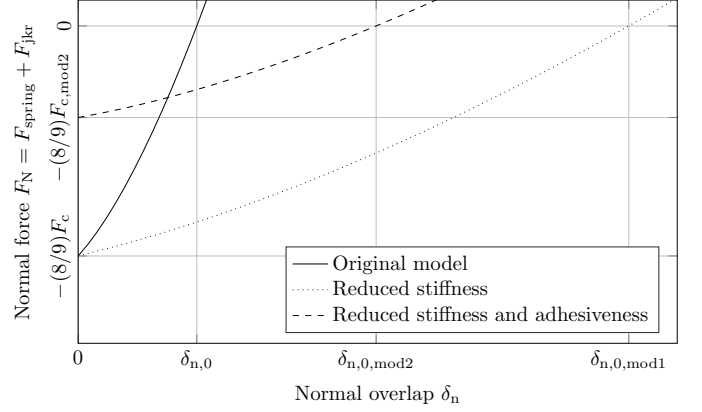

Figure 3: Comparison of force-displacement relations using the original JKR model and different modified versions: —— Original Hertz and JKR model [1]; ······ Reduced Young's modulus but unaltered surface energy density; - - - - Reduced Young's modulus and modified surface energy density given by the criterion in equation (24).

constant, the following criterion has to be fulfilled:

$$\int_0^{\delta_{\mathrm{n,0}}} \left(F_{\mathrm{jkr}} + F_{\mathrm{spring}} \right) \mathrm{d}\delta_{\mathrm{n}} = \\ \int_0^{\delta_{\mathrm{n,0,mod}}} \left(F_{\mathrm{jkr,mod}} + F_{\mathrm{spring,mod}} \right) \mathrm{d}\delta_{\mathrm{n}} \tag{23}$$

where $\delta_{\mathrm{n,0}} = (1/3) a_0^2 / R$ is the normal overlap at equilibrium. Inserting expressions for F_{jkr} and F_{spring} from equation (8) and (9) with the contact radius given by equation (10) into equation (23) gives an expression for the modified surface energy density as a result of modified effective Young's modulus:

$$\gamma_{\mathrm{mod}} = \gamma \left(\frac{E_{\mathrm{mod}}}{E} \right)^{2/5} \tag{24}$$

Details on how this derived from (23) are given in appendix A. The result in (24) is actually the same criterion Gu et al. [8] found for the contact independent van der Waals formulation [16] $F_{\mathrm{vdW}} = A_{\mathrm{H}} R / (6 D_{\mathrm{min}}^2)$ with the effective Hamaker constant $A_{\mathrm{H}} = 24 \pi D_{\mathrm{min}}^2 \gamma$. Figure 3 shows a comparison of the original JKR model, the JKR model with reduced particle stiffness and the JKR model with reduced particle stiffness and reduced surface energy density using equation (24). As the figure shows, by only reducing the particle stiffness (by the Young's modulus E) the same force ($F_{\mathrm{N}} = -(8/9) F_{\mathrm{C}}$) is required to break contact. However, the equilibrium overlap is increased significantly as $\delta_{\mathrm{N,0,mod}} = (1/3) a_{0,\mathrm{mod}}^2 / R = (3 \pi^2 \gamma^2 R / E_{\mathrm{mod}}^2)^{1/3}$. By reducing both the stiffness and adhesiveness (by the surface energy density γ) using equation (24), the force-displacement relation is changed so that the separation energy remains the same as in the original model. The result is a higher overlap distances during collision and consequently larger time step sizes. However, the normal force required to break contact is reduced to
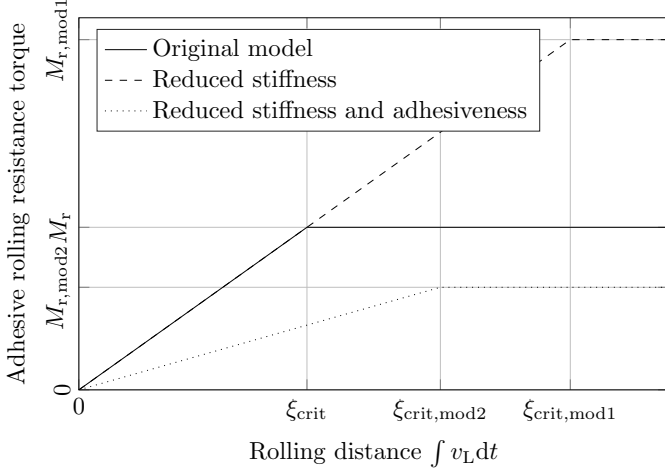
Figure 4: Comparison of torque-rolling distance relations using the original JKR model and different modified versions: —— Original adhesive rolling resistance torque model by [2–4]; ⋯⋯ Reduced Young's modulus but unaltered surface energy density; - - - - Reduced Young's modulus and modified surface energy density given by the criterion in equation (24).

$F_N = -(8/9)F_{C,mod} = -(8/9)3\pi R\gamma_{mod}$. This can pose some impracticalities for systems with large external forces acting to separate the particles. This is discussed further in section 6.

3.2. Modified adhesive rolling torque model for reduced particle stiffness

In the prediction of particle deposition, the adhesive rolling resistance model acts to stop particles from rolling on a surface even when a constant external force is applied parallel to the surface. When introducing a reduced particle stiffness model, it is important that the particles will deposit predicted by the original model.

When a reduced particle stiffness is introduced in the rolling torque model, the equilibrium contact radius a_0 in (7) is increased. As a consequence, the critical rolling displacement distance in (18) is increased as well causing particles to roll a longer distance before beginning to roll irreversibly with constant rolling resistance torque opposing rolling. This is shown in figure 4, which shows the rolling torque on particles in normal equilibrium with a surface ($a = a_0$) affected by constant external force. Likewise, if both the particle stiffness and adhesiveness are reduced using (24), both the critical rolling distance and the critical rolling torque are changed as shown in figure 4 as well.

Therefore, the only way to retain the behaviour of the original model is to keep all terms but the $(a/a_0)^{3/2}$ term unaltered. The $(a/a_0)^{3/2}$ term is modified to include modified values for the instantaneous and equilibrium contact radii, so that $(a/a_0)^{3/2}$ is replaced by $(a_{mod}/a_{0,mod})^{3/2}$.

In that way, particles have the same behaviour when in normal equilibrium with a surface as in the original model but uses modified values before equilibrium is established.

It should be noted that as a natural consequence of introducing a reduced particle stiffness, the particles will travel longer distances upon collision due to the changed force-displacement relation, see figure 3. When collisions with a plane wall at an oblique angle are considered, the result is particles travelling a slightly longer distance before coming to rest. However, this is typically not of importance in DEM simulations involving many particles.

4. Validation by Experimental Data

Collisions of small spheres have been studied thoroughly. At sufficiently low impact velocities, the collisions are dominated by adhesive forces in the contact region resulting in sticking behaviour, where the effective coefficient of restitution e_{eff} is zero. At higher impact velocities when the particles are unable to stick, the effective coefficient of restitution increases rapidly with increasing impact velocity. At sufficiently high velocities where the collisions become increasingly unaffected by adhesive forces, the effective coefficient of restitution approaches the coefficient of restitution e.

In the following, simulation results obtained by integrating (3) for both non-modified and modified stiffness using (24) are compared to experimental data presented by Dahneke [27]. As noted by Krijt et al. [28], expected collision outcomes typically differ slightly from experiments as even small imperfections in particle or wall material result in a non-perfect collision. Therefore, the fitted values suggested by Krijt et al. [28] are used when comparing to experiments. Figure 5 shows how the simulation results with both non-modified and modified stiffnesses compare to experimental data.

Figure 5 shows that the DEM methodology described above is capable of predicting the effective coefficient of restitution. Furthermore, by reducing the particle stiffness from E to E_{mod} and modifying the surface energy density by analytical solution in (24), the exact same results are indeed obtained. More details on how introducing softer particles allows for a higher time step size are given in section 6.

5. Test Cases

5.1. Dimensionless quantities

To generalise the analysis, particle properties are reported based on a set of dimensionless quantities that control different aspects of the adhesion and rolling processes, which ultimately govern the agglomeration and deposition processes. Based on the effective Young's modulus E, effective radius R, relative particle velocity before impact v, particle density ρ_p, collision angle ψ, and coefficient of restitution e, the adhesion process is fully described. The above mentioned parameters form three governing parameters: an elasticity parameter describing the ratio between particle stiffness and particle
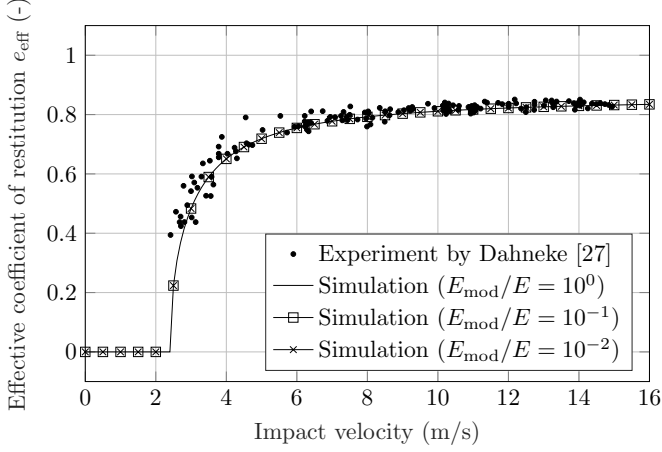
Figure 5: Comparison to experiment by Dahneke [27] with PSL spheres colliding with a plane wall of polished quartz. Collision properties are $d_{\mathrm{p}} = 1.27$ μm, $E = 271$ MPa, $\gamma = 0.11$ J/m^2, $\rho_{\mathrm{p}} = 1026$ kg/m^3 and $e = 0.86$ (fitted to experimental data at high velocities), see Krijt et al. [28] and supplementary online material for collision properties. When a reduced particle stiffness is introduced in the simulations, the surface energy density is modified using the criterion proposed in (24).

inertia $\lambda = E/(\rho_{\mathrm{p}}v^2)$, an adhesiveness parameter describing the ratio between particle adhesiveness and particle inertia $\mathrm{Ad} = 3\gamma/(\rho_{\mathrm{p}}v^2r_{\mathrm{i}}) \cdot (1+\beta^3)/((1+\beta^2)\beta)$ [29], and the effective coefficient of restitution describing the ratio between relative velocity after collision (subscript f) and before collision $e_{\mathrm{eff}} = (v_{\mathrm{i,f}} - v_{\mathrm{j,f}})/(v_{\mathrm{j}} - v_{\mathrm{i}})$. To describe the effect of adhesiveness on the collision, the coefficient of restitution is reported as a scaled value between 0 and 1, giving the ratio between the effective and the non-adhesive coefficient of restitution $\hat{e} = e_{\mathrm{eff}}/e$. In the case of collision with a wall at an oblique angle ψ, the collision angle is accounted for in the elasticity parameter and adhesiveness parameter, so that $\lambda = E/\left(\rho_{\mathrm{p}}v^2\sin^2\psi\right)$ and $\mathrm{Ad} = 3\gamma/(\rho_{\mathrm{p}}v^2\sin^2(\psi)r_{\mathrm{i}}) \cdot (1+\beta^3)/((1+\beta^2)\beta)$. In the case of particle-wall collisions, the adhesiveness parameter reduces to $\mathrm{Ad} = 3\gamma/(\rho_{\mathrm{p}}v^2\sin^2(\psi)r_{\mathrm{p}})$, where r_{p} is the particle radius.

To describe adhesive rolling, the adhesion hysteresis parameter $\Delta\gamma/\gamma$ is used as well. To describe adhesion followed by rolling on a plane wall, the external force is made non-dimensional by the yield force required to overcome the critical rolling resistance torque, forming $\hat{F} = F_{\mathrm{ext}}/F_{\mathrm{yield}}$, where $F_{\mathrm{yield}} = M_{\mathrm{r}}/R$. In the case of normal equilibrium $a = a_0$, the yield force reduces to $F_{\mathrm{yield}} = 4F_{\mathrm{C}}a_0(\Delta\gamma/\gamma)/12$. That is, $\hat{F} < 1$ describes processes where particles eventually come to a halt due to adhesive forces in the contact region. Likewise, $\hat{F} \geq 1$ describes rolling processes where particles will keep rolling regardless of the adhesive rolling resistance torque. The effective coefficient of restitution e_{eff} of an adhesive collision processes is generally lower than that of a non-adhesive collision e.
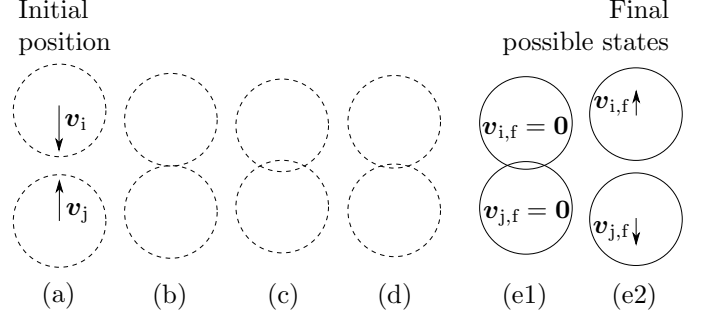

Figure 6: Overview of the different stages of a particle-particle collision: (a) Particles approaching each other; (b) Just prior to contact the particles are still unaffected and move with velocity $\boldsymbol{v}$; (c) particles reach maximum normal overlap δ_{n}; (d) Particles begin to separate; (e1-e2) Depending on the strength of the adhesive force the particles will either remain in contact (e1) or separate completely (e2).
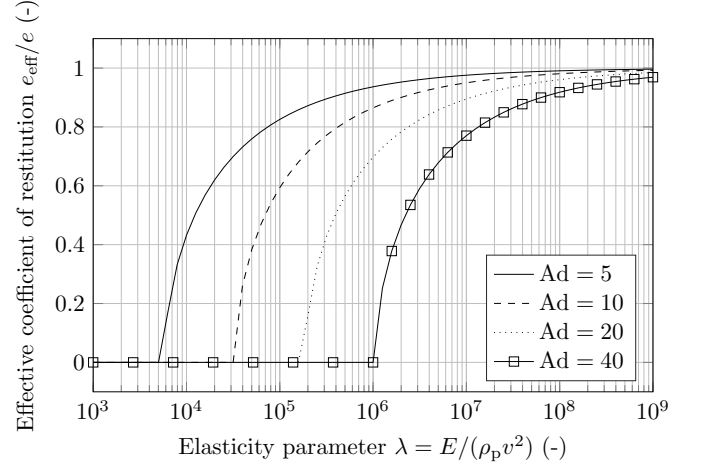

Figure 7: Numerical simulations showing head-on particle-particle adhesive collisions by the non-modified model showing the effective coefficient of restitution as function of the elasticity parameter at various adhesive parameters $\mathrm{Ad} = \gamma/(\rho_{\mathrm{p}}v^2R)$ for a coefficient of restitution $e = 0.3$.

5.2. Binary Adhesive Collision

Binary particle collisions are encountered in most problems being solved using the DEM method. Therefore it is important that the model proposed for reduced particle stiffness simulations yields similar results for particle collisions. This is investigated in the following with figure 6 giving an overview of the head-on particle-particle collision being simulated to validate the proposed model. By varying the elasticity parameter λ and the adhesiveness parameter Ad, the particles either stay attached, as in figure 6(e1), or separate with velocity $\boldsymbol{v}_{\mathrm{f}}$ as in figure 6(e2). Figure 7 shows how variations in elasticity parameter at different adhesiveness parameter affect the effective coefficient of restitution. The figure shows how the particles stay attached below a certain critical elasticity parameter. This critical elasticity parameter depends on the adhesiveness parameter and increases with increasing adhesiveness parameter. As the results show, decreasing the particle stiffness does, in most cases, result in a
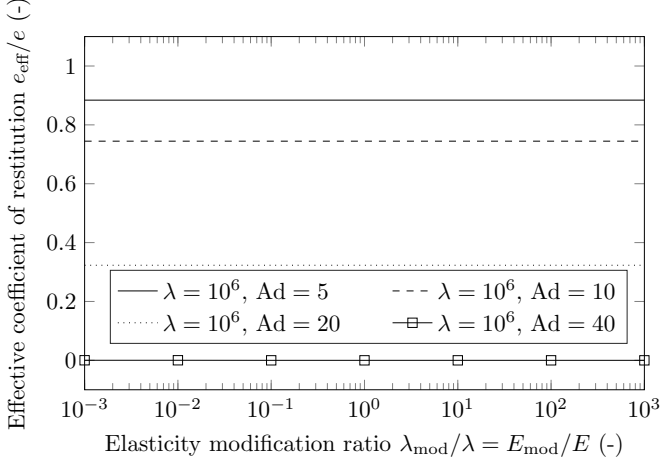
Figure 8: Numerical simulation showing head-on particle-particle adhesive collisions showing how the effective coefficient of restitution remains constant when the particle stiffness is reduced (or increased) when the surface energy density is changed using the criterion proposed in (24). Again, results are shown for coefficient of restitution $e = 0.3$.

different effective coefficient of restitution. The exception is at sufficiently low elasticity parameters, where the particle stay attached upon collision. Furthermore, the figure shows that as long as $e_{\mathrm{eff}}/e \approx 1$, corresponding to high elasticity parameters, the elasticity parameter can be reduced with only small changes in effective coefficient of restitution as the collision behaves as non-adhesive.

Figure 8 shows how using the criterion in (24) makes the effective coefficient of restitution independent of changes in elasticity parameter from a base value $\lambda = 10^6$. As figure 8 shows, the effective coefficient of restitution e_{eff}/e retains the values from $\lambda = 10^6$ in figure 7 when the elasticity parameter is changed at various adhesiveness values. Even though the stiffness of particles undergoing binary particle-particle collisions can be greatly reduced, studies by Kobayashi et al. [9] and Gu et al. [8] show that collisions involving larger agglomerates behave differently when the particle stiffness is reduced beyond a certain point. In this study, this phenomenon is addressed in the following section where particle deposition on both a clean surface and a surface with an initial layer of particles is investigated.

5.3. Deposition on a Plane Surface

Most problems being solved using DEM involve particles colliding with a plane surface. This case is different from the previous head-on particle collisions as particles may roll on the surface or other particles and eventually come to rest due to adhesive rolling resistance torque described by equation (21). Therefore, this section is focused on the validity of the proposed model for particles with reduced stiffness colliding with a plane surface. Figure 9 gives an overview of the oblique angle particle-wall collision process investigated.
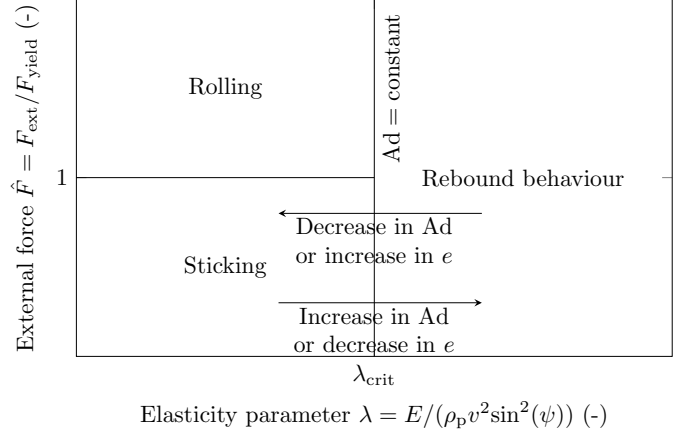

Figure 10: The three possible outcomes of an adhesive collision with a plane wall and the effect of increasing/decreasing adhesiveness parameter $\mathrm{Ad} = 3\gamma/(\rho_{\mathrm{p}} v^2 \sin^2(\psi) r_{\mathrm{p}})$ and coefficient of restitution e. The particle is affected by a constant external force F_{ext} parallel to the wall (see figure 9) and the yield force is given by $F_{\mathrm{yield}} = 4 F_{\mathrm{C}} a_0 (\Delta\gamma/\gamma)/12$.
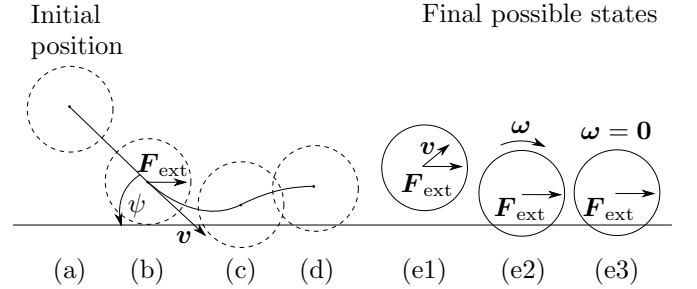

Figure 9: Overview of the different stages of the particle-wall collision: (a) The particle moving towards the wall; (b) Just prior to contact the particle is still unaffected by the wall and moves with velocity v at an angle ψ to the wall while affected by an external fluid/gravity force F_{ext}; (c)-(d) Particle in contact with the wall. If the particle stay in contact with the wall, the normal equilibrium is established here; (e1-e3) The particle will either rebound and move away from the surface (e1), stay at the surface but keep rolling with a constant angular velocity $\omega \neq 0$ (e2) or stay in place as a result of adhesiveness with shifted centre of contact and centre of mass $\omega = 0$ (e3), see figure 2(b).

As the figure shows, three possible outcomes are expected as collision parameters are varied: rebound behaviour, particle deposition followed by rolling motion and particle deposition where the particle rolls a certain distance before coming to a halt. For most DEM simulations of particulate deposition, it is important that the outcome (rebound, rolling or sticking) remains the same when the particle stiffness is reduced. Simulations of particles colliding with a wall at oblique angles $\psi \in \ ]0; \pi/2]$ were done. The three possible outcomes are located as shown in the dimensionless map in figure 10, where elasticity and adhesiveness parameter are modified to account for the collision angle ψ so that: $\lambda = E/(\rho_{\mathrm{p}} v^2 \sin^2 \psi)$ and $\mathrm{Ad} = 3\gamma/(\rho_{\mathrm{p}} v^2 \sin^2(\psi) r_{\mathrm{p}})$. A high elasticity parameter, high coefficient of restitution or low adhesiveness parameter will all inherently cause the particles to rebound. When the particles stay attached
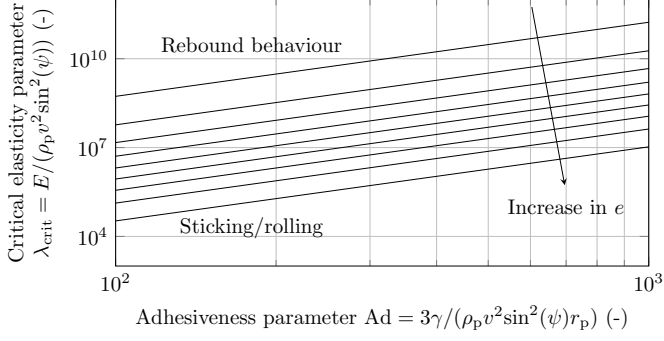
Figure 11: The critical elasticity parameter describing the border between sticking/rolling and rebound behaviour from figure 10. Lines indicate increasing coefficient of restitution e from 0.1 to 0.9 at intervals of 0.1 as indicated by the arrow.
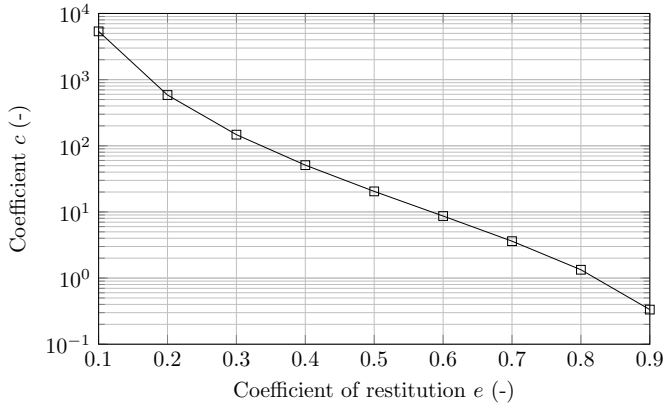

Figure 12: Coefficient c in equation (25) as function of coefficient of restitution e.

to the wall, the external force $\hat{F}$ dictates if the particles stay in place due to adhesiveness ($\hat{F} < 1$) or keep rolling ($\hat{F} \geq 1$).

To find the critical elasticity parameter causing particles to rebound from figure 10, the bisection algorithm is used with convergence criterion $|\delta_n/r_p| = 10^{-7}$. Figure 11 shows the critical elasticity parameter as function of adhesiveness parameter at various coefficients of restitution. All the lines of constant coefficient of restitution in figure 11 follow the equation:

$$\lambda_{\text{crit}} = c \cdot \text{Ad}^{5/2} \tag{25}$$

where the value of c is solely a function of the coefficient of restitution e as shown in figure 12. That is, the above equation can be used to find the critical elasticity parameter giving the border between rebound and sticking behaviour.

6. Summary and discussion

6.1. Summary

A method has been presented for reducing the particle stiffness for DEM simulations using a Hertzian approach

to predict collisions of adhesive micron-sized particles for which the adhesive model by Johnson-Kendall-Roberts (JKR) model is applicable. The following conclusions can be drawn:

- When using the simplified JKR model (equation (8)), the particle Young's modulus can be reduced from E to E_{mod} as long as the surface energy density is reduced as well using $\gamma_{\text{mod}} = \gamma(E_{\text{mod}}/E)^{2/5}$. That way, the border between sticking and rebounding behaviour remains the same when the particle stiffness is reduced.

- To use the rolling resistance model by Dominik and Tielens [2, 3], Krijt et al. [4] (equation (18) to (22)) for reduced particle stiffness simulations, only the term $(a/a_0)^{3/2}$ should be changed to use modified values. That way, the border between rolling and sticking remains the same. As a natural result of the reduced particle stiffness, the particles will travel a longer distance before the equilibrium condition is reached.

6.2. Discussion on computational time and limitations

As the particle stiffness is reduced, the time step size can be greatly increased. Figure 13 shows the velocity during a collision of a small PSL sphere impacting a polished quartz surface, corresponding to the experiment by Dahneke [27].

As the figure shows, the separation velocity is unaffected by a change in particle stiffness when the surface energy density is modified using (24). However, the particle collision process now takes place over significantly longer time periods. When resolving a collision over fixed number of time steps (Silbert et al. [30] suggests $\Delta t_{\text{col}}/\delta t \approx 50$), the time step size can now be greatly increased. By looking at how the collision time Δt_{col} scales with a reductions in particles stiffness, it is found that $\Delta t_{\text{col,mod}} = \Delta t_{\text{col}}(E/E_{\text{mod}})^{2/5}$, see figure 13. This criterion can be used to estimate the possible speed-up for adhesive DEM simulations when introducing a reduced particle stiffness.

As a consequence of a reduced particle stiffness, the critical force required to separate two agglomerated particles is reduced as well. This fact is important when simulating particles in flow or magnetic fields where local external forces on particles can be strong. A such example could be a strong shear flow field. Therefore, care should be taken when introducing reduced particle stiffness to make sure that the critical force $F_{\text{C}} = 3\pi R \gamma_{\text{mod}}$ still remains significantly higher than typical external forces trying to separate the particles.

Additionally, it should be noted that for collisions involving many particles with a local volume fraction approaching the closed-pack solution, the adhesive behaviour might be changed slightly if the particle stiffness is reduced too much, $E_{\text{mod}}/E < 10^{-3}$ [8, 9].
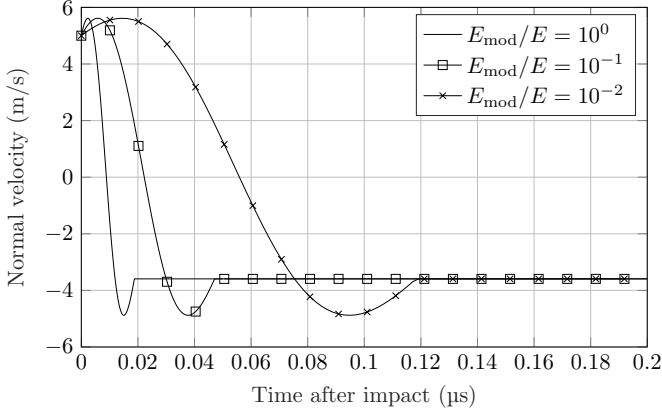
Figure 13: Velocity as function of time during a collision for a PSL sphere colliding with a polished quartz wall with an impact velocity of 5 m/s. When the particle stiffness is reduced from $E_{\text{mod}}/E = 10^0$ to $E_{\text{mod}}/E = 10^{-1}$ and $E_{\text{mod}}/E = 10^{-2}$, the surface energy density is modified using the criterion proposed in (24).

Acknowledgement

Appendix A. Details on derivation of the criterion in (24)

Instead of deriving (24) from (23) directly, we use integration by substitution to rewrite (23) in terms of contact radius a instead of normal overlap δ_{n}:

$$\int_{a(\delta_{\text{n}}=0)}^{a(\delta_{\text{n}}=\delta_{\text{n},0})} (F_{\text{jkr}} + F_{\text{spring}})\, \mathrm{d}a = \\ \int_{a(\delta_{\text{n}}=0)}^{a(\delta_{\text{n}}=\delta_{\text{n},0,\text{mod}})} (F_{\text{jkr,mod}} + F_{\text{spring,mod}})\, \mathrm{d}a \quad \text{(A.1)}$$

Next, expressions for the contact radius at $\delta_{\text{n}} = 0$, $\delta_{\text{n}} = \delta_{\text{n},0}$ and $\delta_{\text{n}} = \delta_{\text{n},0,\text{mod}}$ are found. The contact radius at zero-overlap is found by isolating a in (10) with $\delta_{\text{n}} = 0$:

$$a^4 - 2R\delta_{\text{n}}a^2 - \frac{4\pi\gamma}{E}R^2 a + R^2\delta_{\text{n}}^2 = 0 \quad \text{(A.2)}$$

The two real roots are:

$$a_1 = 0 \quad \text{(A.3)}$$

$$a_2 = \left(\frac{4\pi\gamma R^2}{E}\right)^{1/3} \quad \text{(A.4)}$$

Here we are interested in the non-zero root a_2, which is the lower limit of the integrals in (A.1):

$$a(\delta_{\text{n}} = 0) = \left(\frac{4\pi\gamma R^2}{E}\right)^{1/3} \quad \text{(A.5)}$$

The upper limits for a at $\delta_{\text{n}} = \delta_{\text{n},0}$ and a at $\delta_{\text{n}} = \delta_{\text{n},0,\text{mod}}$ are the equilibrium contact radius given directly by (7):

$$a(\delta_{\text{n}} = \delta_{\text{n},0}) = \left(\frac{9\pi\gamma R^2}{E}\right)^{1/3} \quad \text{(A.6)}$$

$$a(\delta_{\text{n}} = \delta_{\text{n},0,\text{mod}}) = \left(\frac{9\pi\gamma_{\text{mod}}R^2}{E_{\text{mod}}}\right)^{1/3} \quad \text{(A.7)}$$

Next, we look for an expression for $\mathrm{d}\delta_{\text{n}}$. First, we derive an expression for $\delta_{\text{n}}(a)$ using (10). We obtain two solutions:

$$\delta_{\text{n},1} = \frac{Ea^2 + 2R\sqrt{E\gamma a\pi}}{ER} \quad \text{(A.8)}$$

$$\delta_{\text{n},2} = \frac{Ea^2 - 2R\sqrt{E\gamma a\pi}}{ER} \quad \text{(A.9)}$$

Here only the solution in (A.9) fulfills the criteria in (A.5) and (A.6). Next, we find the derivative $\mathrm{d}\delta_{\text{n}}/\mathrm{d}a$ using (A.9) and isolate for $\mathrm{d}\delta_{\text{n}}$:

$$\mathrm{d}\delta_{\text{n}} = \left(\frac{2a}{R} - \frac{2\sqrt{\gamma\pi}}{\sqrt{Ea}}\right)\mathrm{d}a \quad \text{(A.10)}$$

Carrying out the integral in (A.1) with the limits given by (A.5), (A.6) and (A.7) and inserting the expression for $\mathrm{d}\delta_{\text{n}}$ from (A.10), we obtain:

$$\frac{\gamma^{5/3}}{E^{2/3}} = \frac{\gamma_{\text{mod}}^{5/3}}{E_{\text{mod}}^{2/3}} \quad \text{(A.11)}$$

which reduces to the expression in (24).

References

[1] K. L. Johnson, K. Kendall, A. D. Roberts, Surface energy and the contact of elastic solids, Proc. R. Soc. Lond. 324 (1971) 301–313, DOI: http://dx.doi.org/10.1098/rspa.1971.0141.

[2] C. Dominik, A. G. G. M. Tielens, Resistance to rolling in the adhesive contact of two elastic spheres, Philosophical Magazine A 72 (1995) 783–803, DOI: http://dx.doi.org/10.1080/01418619508243800.

[3] C. Dominik, A. G. G. M. Tielens, The Physics of Dust Coagulation and the Structure of Dust Aggregates in Space, The Astrophysical Journal 480 (1997) 647–673, DOI: http://dx.doi.org/10.1086/303996.

[4] S. Krijt, C. Dominik, A. G. G. M. Tielens, Rolling friction of adhesive microspheres, Journal of Physics D: Applied Physics 47 (2014) 175302 (9pp), DOI: http://dx.doi.org/10.1088/0022-3727/47/17/175302.

[5] E. Barthel, Adhesive elastic contacts: JKR and more, Journal of Physics D: Applied Physics 41 (2008) 163001 (20pp), DOI: http://dx.doi.org/10.1088/0022-3727/41/16/1630.

[6] C. Henry, J.-P. Minier, G. Lefèvre, Towards a description of particulate fouling: From single particle deposition to clogging, Advances in Colloid and Interface Science 185–186 (2012) 34–76, DOI: http://dx.doi.org/10.1016/j.cis.2012.10.001.

[7] Y. Tsuji, T. Kawaguchi, T. Tanaka, Discrete element simulation of two-dimensional fluidized bed, Powder Technology 77 (1993) 79–87, DOI: http://dx.doi.org/10.1016/0032-5910(93)85010-7.

[8] Y. Gu, A. Ozel, S. Sundaresan, A modified cohesion model for CFD-DEM simulations of fluidization, Powder Technology 296 (2016) 17–28, DOI: http://dx.doi.org/10.1016/j.powtec.2015.09.037.

[9] T. Kobayashi, T. Tanaka, N. Shimada, T. Kawaguchi, DEM-CFD analysis of fluidization behavior of Geldart Group A particles using a dynamic adhesion force model, Powder Technology 248 (2013) 143–152, DOI: http://dx.doi.org/10.1016/j.powtec.2013.02.028.

[10] K. L. Johnson, J. A. Greenwood, An Adhesion Map for the Contact of Elastic Spheres, Journal of Colloid and Interface Science 192 (1997) 326–333, DOI: http://dx.doi.org/10.1006/jcis.1997.4984.

[11] D. Tabor, Surface Forces and Surface Interactions, Journal of Colloid and Interface Science 58 (1975) 2–13, DOI: http://dx.doi.org/10.1016/0021-9797(77)90366-6.

[12] J. N. Israelachvili, Intermolecular and Surface Forces, Academic Press, 2. edn., iSBN: 978-0-12-375182-9, 1992.

[13] E. J. R. Parteli, J. Schmidt, C. Brümel, K.-E. Wirth, W. Peukert, T. Pöschel, Attractive particle interaction forces and packing density of fine glass powders, Nature Scientific Reports 4 (2014) 1–7, DOI: http://dx.doi.org/10.1038/srep06227.

[14] B. V. Derjaguin, V. M. Muller, Y. P. Toporov, Effect of Contact Deformations on the Adhesion of Particles, Journal of Colloid and Interface Science 53 (1975) 314–356, DOI: http://dx.doi.org/10.1016/0079-6816(94)90044-2.

[15] D. Maugis, Adhesion of Spheres: The JKR-DMT Transition Using a Dugdale Model, Journal of Colloid and Interface Science 150 (1992) 243–269, DOI: http://dx.doi.org/10.1016/0021-9797(92)90285-T.

[16] H. C. Hamaker, The London - Van der Waals Attraction between Spherical Particles, Physica IV 10 (1937) 1058–1072, DOI: http://dx.doi.org/10.1016/S0031-8914(37)80203-7.

[17] H. Abbasfard, G. Evans, R. Moreno-Atanasio, Effect of van der Waals force cut-off distance on adhesive collision parameters in DEM simulation, Powder Technology 299 (2016) 9–18, DOI: http://dx.doi.org/10.1016/j.powtec.2016.05.020.

[18] F. Chaumeil, M. Crapper, Using the DEM-CFD method to predict Brownian particle deposition in a constrained tube, Particuology 15 (2014) 94–106, DOI: http://dx.doi.org/10.1016/j.partic.2013.05.005.

[19] J. S. Marshall, Particle aggregation and capture by walls in a particulate aerosol channel flow, Aerosol Science 38 (2007) 333–351, DOI: http://dx.doi.org/j.jaerosci.2007.01.004.

[20] J. S. Marshall, Discrete-element modelling of particulate aerosol flows, Journal of Computational Physics 228 (2009) 1541–1561, DOI: http://dx.doi.org/j.jcp.2008.10.035.

[21] M. Pasha, C. Hare, A. Hassanpour, M. Ghadiri, Analysis of ball indentation on cohesive powder beds using distinct element modelling, Powder Technology 233 (2013) 80–90, DOI: http://dx.doi.org/10.1016/j.powtec.2012.08.017.

[22] X. Deng, J. V. Scicolone, R. N. Davé, Discrete element method simulation of cohesive particles mixing under magnetically assisted impaction, Powder Technology 243 (2013) 96–109, DOI: http://dx.doi.org/10.1016/j.powtec.2013.03.043.

[23] A. Chokshi, A. G. G. M. Tielens, D. Hollenbach, Dust Coagulation, The Astrophysical Journal 407 (1993) 806–819, DOI: http://dx.doi.org/10.1086/172562.

[24] C. Thornton, Interparticle sliding in the presence of adhesion, Journal of Physics D: Applied Physics 24 (1991) 1942–1946, DOI: http://doi.org/10.1088/0022-3727/24/11/007.

[25] C. Thornton, K. K. Yin, Impact of elastic spheres with and without adhesion, Powder Technology 65 (1991) 153–166, DOI: http://dx.doi.org/10.1016/0032-5910(91)80178-L.

[26] M. Oda, J. Konishi, S. Nemat-Nasser, Experimental micromechanical evaluation of strength of granular materials: Effects of particle rolling, Mechanics of Materials 1 (1982) 269–283, DOI: http://dx.doi.org/10.1016/0167-6636(82)90027-8.

[27] B. Dahneke, Further Measurements of the Bouncing of Small Latex Spheres, Journal of Colloid and Interface Science 51 (1975) 58–65, DOI: http://doi.org/10.1016/0021-9797(75)90083-1.

[28] S. Krijt, G. Güttler, D. Heißelmann, C. Dominik, A. G. G. M. Tielens, Energy dissipation in head-on collisions of spheres, Journal of Physics D: Applied Physics 46 (2013) 435303, DOI: http://doi.org/10.1088/0022-3727/46/43/435303.

[29] S. Chen, S. Li, M. Yang, Sticking/rebound criterion for collisions of small adhesive particles: Effects of impact parameter and particle size, Powder Technology 274 (2015) 431–440, DOI: http://dx.doi.org/10.1016/j.powtec.2015.01.051.

[30] L. E. Silbert, D. Ertas, G. S. Grest, T. C. Halsey, D. Levine, S. J. Plimpton, Granular flow down an inclined plane: Bagnold scaling and rheology, Physical Review (2001) 051302DOI: http://dx.doi.org/10.1103/PhysRevE.64.051302.

Nomenclature

Ad	adhesiveness parameter (-)
A_{H}	effective Hamaker constant (J)
a	contact radius (m)
d_{p}	particle diameter (m)
$D_{\min}$	minimum separation distance (m)
E (no subscripts)	effective Young's modulus (Pa)
$E_{\mathrm{i}}, E_{\mathrm{j}}$	Young's modulus for particle i, j (Pa)
e	coefficient of restitution (-)
$\boldsymbol{F}$	force (N)
F_{C}	critical force (N)
I	particle moment of inertia (kg m^2)
k	spring constant (N m^{-1})
k_{r}	rolling stiffness (N)
M	particle torque (Nm)
m (no subscripts)	effective particle mass (kg)
$m_{\mathrm{i}}, m_{\mathrm{j}}$	particle mass for particle i, j (kg)
$\boldsymbol{n}$	normal unit vector (-)
R	effective particle radius (m)
r_{p}	particle radius (m)
$r_{\mathrm{i}}, r_{\mathrm{j}}$	particle radius for particle i,j (m)
S	damping force coefficient (kg s^{-2})
t	time (s)
$\boldsymbol{v}$	relative velocity (m s^{-1})
$\boldsymbol{v}_{\mathrm{L}}$	relative rolling velocity (m s^{-1})
$\boldsymbol{v}_{\mathrm{S}}$	slip velocity (m s^{-1})
$\boldsymbol{x}$	particle position (m)

Greek letters

β	coefficient used for damping force (-)
$\Delta\gamma/\gamma$	adhesion hysteresis value (-)
Δt_{col}	time period for oscillations or collision (s)
δt	collision time step size (s)
δs_{t}	tangential displacement (m)
δ	normal overlap (m)
γ	surface energy density (J m^{-2})
λ	elasticity parameter (-)
λ_{T}	Tabor parameter (-)
μ_{s}	sliding friction coefficient (-)
ν	Poisson's ratio (-)
ϕ	adhesiveness parameter (-)
ρ_{p}	particle density (kg m^{-3})
ψ	collision angle (-)
ω	particle angular velocity (s^{-1})
ξ	rolling displacement (m)

Subscripts

0	equilibrium condition
ad	adhesive
crit	critical
con	contact
damp	damping
eff	effective
ext	external
f	final
mod	modified values
i	particle i
j	particle j
n	normal direction
r	rolling resistance
t	tangential direction
vdW	van der Waals

Acronyms

DEM	Discrete Element Modelling
DMT	Derjaguin-Muller-Toporov model
JKR	Johnson-Kendall-Roberts model